Biochemical and Biophysical Research Communications 385 (2009) 88–93

Contents lists available at ScienceDirect

Biochemical and Biophysical Research Communications

journal homepage: www.elsevier.com/locate/ybbrc

Single-fluorophore monitoring of DNA hybridization for investigating the effect of secondary structure on the nucleation step

Joon-Jung Jo, Min-Ji Kim, Jung-Tae Son, Jandi Kim, Jong-Shik Shin *

Department of Biotechnology, Yonsei University, Shinchon-Dong 134, Seodaemun-Gu, Seoul 120-749, South Korea

ARTICLE INFO

Article history:
Received 1 April 2009
Available online 5 May 2009

Keywords:
DNA oligonucleotide
Hybridization kinetics
Single-fluorophore measurement
Secondary structure
Nucleation
Activation energy
Salt dependence

ABSTRACT

Nucleic acid hybridization is one of the essential biological processes involved in storage and transmission of genetic information. Here we quantitatively determined the effect of secondary structure on the hybridization activation energy using structurally defined oligonucleotides. It turned out that activation energy is linearly proportional to the length of a single-stranded region flanking a nucleation site, generating a 0.18 kcal/mol energy barrier per nucleotide. Based on this result, we propose that the presence of single-stranded segments available for non-productive base pairing with a nucleation counterpart extends the searching process for nucleation sites to find a perfect match. This result may provide insights into rational selection of a target mRNA site for siRNA and antisense gene silencing.

Introduction

Nucleic acid hybridization based on Watson–Crick base-pair complementarity underlies a number of essential biological processes such as genetic information storage and transmission [1], three-dimensional folding of nucleic acids [2] and genetic regulation by non-coding RNA elements [3]. Mechanism-based understanding of the hybridization process is a prerequisite to elucidation of the relevant biological phenomena. In addition to the biological implications, recent advent of new technologies involving short oligonucleotides leads one to pay increasing attention to kinetics and thermodynamics of the nucleic acid hybridization. Typical examples are nucleic acid-based biosensors and microarrays [4,5]. In these applications, predesigned secondary structures of oligonucleotides are often coupled to dynamic functionality of the resulting devices [2]. For example, hairpin structures of molecular beacons ensure spatial proximity of end-labeled fluorophores until a complementary counterpart to a loop region separates the fluorophores by formation of a rigid duplex [6,7]. This example clearly indicates that improving performance of the nucleic acid-based devices requires a thorough understanding on how secondary structures affect hybridization kinetics.

It is generally accepted that nucleic acid hybridization is initiated by formation of a nucleation complex in which stable intermolecular base pairing between complementary regions is formed with a length of a few base pairs [1]. The nucleation complex undergoes zipping-up of unpaired regions, completing the hybridization process [8–10]. The two-step model successfully explained the hybridization kinetics for unstructured oligonucleotides (i.e., devoid of intramolecular secondary structures) [11–14]. In the case of hybridization between structured oligonucleotides, the zipping-up step involves local disruption of intramolecular base pairing. Therefore, hybridization kinetics becomes more complicated than the one for unstructured oligonucleotides. A kinetic model, to our knowledge, is not yet available to predict the effect of secondary structures on the hybridization kinetics [8–10]. To develop a reliable kinetic model, it is essential to understand how the nucleation step is influenced by intramolecular secondary structures. In this study, we have attempted to address the issue using structurally defined oligonucleotides with a varying length of a single-stranded overhang segment close to a nucleation site.

To this end, an accurate detection method should be employed to monitor the progress of hybridization reaction. Monitoring nucleic acid hybridization has been carried out using absorbance hypochromicity [15–17], fluorescence resonance energy transfer (FRET) [8,9,13,14,18–21] and surface plasmon resonance (SPR) [10,22,23]. However, there is an intrinsic drawback of these approaches that changes in the detection signal result not only from the final hybridization product but also from hybridization intermediates contributing to early detection signal. To achieve accurate kinetic analysis, it is desirable to use a detection method of which signal changes are only caused by accumulation of the final product. In this study, we monitored DNA hybridization by

* Corresponding author. Fax: +82 2 362 7265.
E-mail address: enzymo@yonsei.ac.kr (J.-S. Shin).

0006-291X/$ - see front matter © 2009 Elsevier Inc. All rights reserved.
doi:10.1016/j.bbrc.2009.04.140

measuring fluorescence changes of a single fluorescent probe end-labeled on one of the two DNA oligonucleotides. Using the single-fluorophore measurement, hybridization rate constants were determined at different temperatures and salt concentrations to investigate the effect of secondary structures on activation energy and change in the number of cations associated in a rate-determining step. From the kinetic measurements, we found that activation energy is directly dependent on the length of a single-stranded overhang that might hinder the nucleation step.

Materials and methods

Synthetic oligonucleotides and secondary structure prediction. HPLC-purified DNA oligonucleotides were purchased from IDT, Inc. (Coralville, USA). Dye labeling of strand O was performed by the supplier. DNA stock solutions (100 μM) were prepared in TE buffer (pH 8.0, 10 mM Tris base, 1 mM EDTA). Sequences for the DNA oligonucleotides were randomly generated and then manually optimized using mfold [24] to minimize undesirable intramolecular secondary structures and unfavorable intermolecular hybridization. DNA secondary structures were predicted by mfold at the conditions of 300 mM NaCl and 298 K. Secondary structure stability (ΔG) was obtained from the mfold calculation.

Kinetic measurements. All the hybridization reactions were performed in a sodium phosphate buffer (50 mM, pH 6.5). Typical reaction conditions were 5 nM strand O and 50 nM strand T (or TN) in the reaction buffer supplemented with 250 mM NaCl (100 μl working volume). Fluorescence measurements were carried out with a fluorometer equipped with a Peltier temperature controller and a photomultiplier detector (PTI Co.). Excitation and emission wavelengths were set to 496 and 517 nm, respectively (both 4 nm bandwidth). Changes in the fluorescence emission were recorded, which were used in curve fitting to a single exponential function.

Kinetic analysis. Pseudo-steady-state reaction conditions were used for kinetic analysis. The kinetic traces obtained from the fluorescence measurements were subjected to curve fitting to determine rate constants (k_{hyb}). Under the reaction conditions (i.e., $[T]_0 \gg [O]_0$ where [T] and [O] represent concentrations of strands T and O, respectively, and subscript 0 represents an initial state), the reaction follows pseudo-first-order kinetics.

$$\frac{d[O]}{dt} = -k_{hyb}[T]_0[O] \quad (1)$$

Integration of Eq. (1) yields a single exponential function whose exponent is linearly proportional to $[T]_0$ (i.e., $k_{obs} = k_{hyb}[T]_0$).

$$[O] = [O]_0 e^{-k_{obs} \cdot t} \quad (2)$$

Because both O and T–O (i.e., the final hybridization product) contribute to fluorescence emission, the total intensity with respect to time is given by

$$f(t) = \varepsilon_{T-O}[T-O] + \varepsilon_O[O], \quad (3)$$

where ε is the molar fluorescence intensity. Because [T–O] equals $[O]_0 - [O]$, Eq. (3) becomes

$$f(t) = \varepsilon_{T-O}[O]_0 + (\varepsilon_O - \varepsilon_{T-O})[O]_0 e^{-k_{obs} \cdot t} \quad (4)$$

Eq. (4) was used for curve fitting to obtain k_{obs} values, and then k_{hyb} values from linear regression between k_{obs} and $[T]_0$.

To determine activation energy, the k_{hyb} values obtained at different temperatures (15–37 °C) were fitted to the Arrhenius equation.

$$\ln k_{hyb} = \ln A - E_a/RT \quad (5)$$

Table 1
DNA sequences for the oligonucleotides to examine effect of hybridization state on the fluorescence intensity.

O	5′-CGATTCAAGCGGTTTGGCGTG-Oregon Green 488-3′
C[a]	5′-CACGCCAAACCGCTTGAATCG-3′
T1[b]	5′-GACTCGCACATCAGTTACCCGCGGAGAGGCTCACGCCAAACCGCTTGAATCG-3′
I	5′-AGCCTCTCCG-3′

[a] Strand C is a perfect complement to strand O.
[b] The single-underlined and double-underlined segments in strand T1 are complementary to strand I and strand O, respectively.

Results

Monitoring DNA hybridization using a single fluorophore

It is known that fluorescence intensity is dependent on hydrophobic environments of a fluorophore [25]. To examine how the hybridization state affects emission intensity of a fluorophore labeled on a DNA oligonucleotide, we measured changes in the fluorescence emission of Oregon Green 488 end-labeled at the 3′-end of strand O upon hybridization with complementary strands shown in Table 1. The fluorescence emission from strand O decreased by 58% at the maximum emission wavelength (λ_{max} = 517 nm) upon formation of a 21-bp duplex with strand C (Fig. 1). Hybridization between strands O and T1 resulted in a 21-bp duplex with a 31-base single-stranded overhang, leading to an increase in fluorescence emission by 31% compared with the O–C duplex. Intriguingly, further hybridization of the O–T1 complex with strand I led to even higher fluorescence emission than that of strand O. In the O–T1–I trimolecular complex, both regions flanking the fluorophore are double-stranded. These results clearly show that emission intensity of a fluorophore labeled on a DNA oligonucleotide is highly sensitive to changes in the local hybridization state. The fluorescence changes shown in Fig. 1 were large enough to allow real-time monitoring of the hybridization reaction, leading us to undertake kinetic measurements using the single fluorophore.

Time-course monitoring of the hybridization reaction between strands O and T1 was carried out by measuring fluorescence intensity of Oregon Green 488 labeled on strand O (Fig. 2). Because of the lower fluorescence emission of the O–T1 complex than that

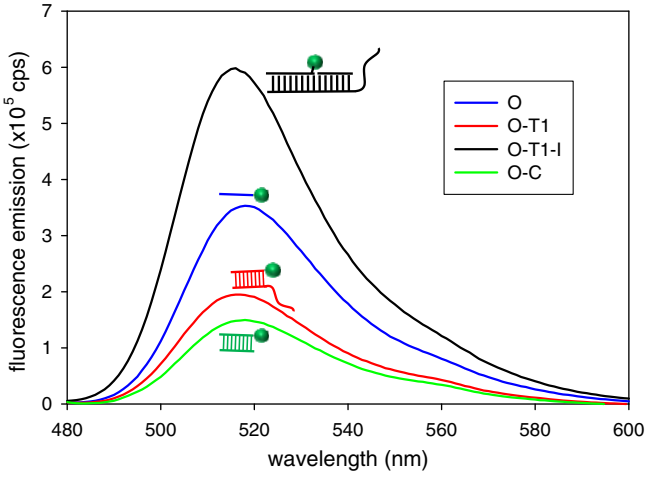

Fig. 1. Changes in fluorescence emission of strand O depending on the hybridization state. Concentrations of the oligonucleotides were 10 nM. Excitation wavelength was set to 470 nm. The green sphere represents Oregon Green 488 labeled at the 3′-end of strand O.

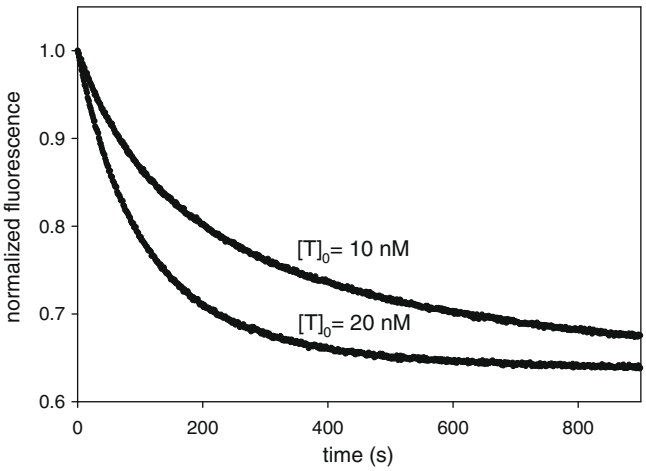

Fig. 2. Kinetic traces for the hybridization reaction between strands O and T1. Concentration of strand O was 10 nM. The reactions were carried out at 21 °C.

of strand O as shown in Fig. 1, the fluorescence intensity decreased as the reaction proceeded. The two kinetic traces were well fitted to a single exponential function, yielding observed kinetic constants of 4.2×10^{-3} and $8.1 \times 10^{-3}\ s^{-1}$ at 10 and 20 nM of strand T1, respectively.

Kinetic measurement with structurally unrelated oligonucleotides

We set out to investigate how secondary structures influence hybridization kinetics using DNA oligonucleotides that are not structurally related. To this end, four additional oligonucleotides of varying length were prepared by successive insertion of randomly generated sequences right before the single-underlined segment of T1 shown in Table 1. The resulting DNA strands from T2 to T5 share a 3′-end 21-base segment complementary to strand O, so the new T strands hybridize with strand O. Secondary structure prediction using mfold showed that no local secondary structures are conserved among the five T strands (see Figure S1 in the Supporting Information). Changes in the free energy for the most stable structures were between −2.9 and −4.8 kcal/mol at room temperature. The mfold calculation predicts that strand O is not capable of forming a stable secondary structure (see Figure S1 in the Supporting Information). The most stable structure is only 0.3 kcal/mol more stable than the structure devoid of any base pairing (note that 0.3 kcal/mol is even lower than the thermal energy RT, i.e. 0.6 kcal/mol).

To obtain hybridization rate constants (k_{hyb}), we used pseudo-steady-state reaction conditions in which concentration of strand T (50–125 nM) was much higher than that of strand O (5 nM). Fig. 3A shows typical kinetic traces, which were fitted to a single exponential function to obtain observed rate constants (k_{obs}). Linear regression between the observed rate constants and the concentrations of strand T is shown in Fig. 3B, yielding k_{hyb} values

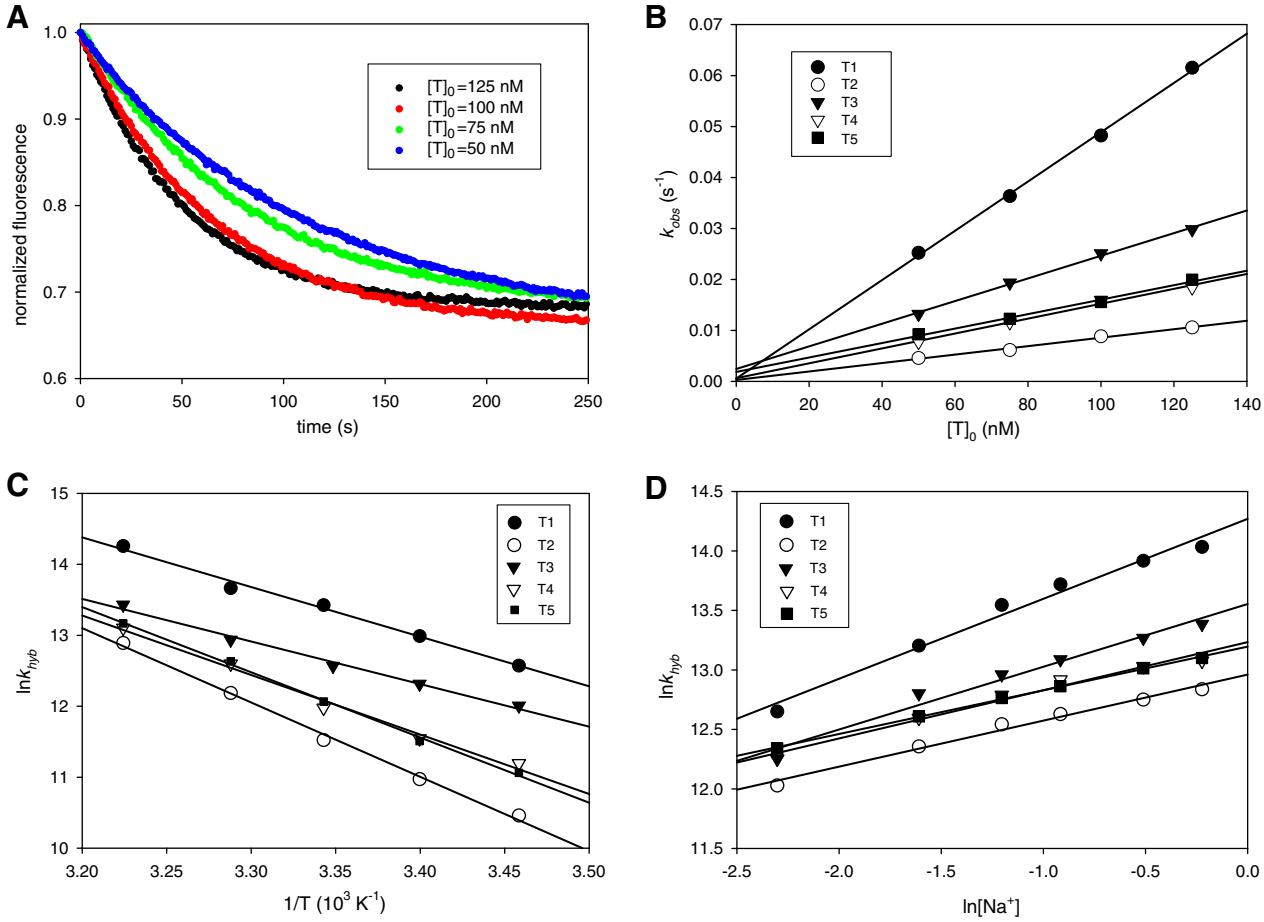

Fig. 3. Kinetic analysis of the hybridization between strands T and O. (A) Typical kinetic traces obtained at 21 °C for hybridization between O and T5 under pseudo-steady-state conditions. Concentration of strand O was 5 nM. (B) Linear relationship between k_{obs} measured at 21 °C and the concentration of strand T. (C) Arrhenius plot to determine activation energy. (D) Salt dependency of the hybridization reaction.

Table 2
Effect of the length of strand T[a] on the hybridization reaction with strand O.

	T1	T2	T3	T4	T5
Oligonucleotide length (nt)	52	57	62	72	82
k_{hyb}[b] (10^5 s^{-1} M^{-1})	15.57 (1.0)[c]	3.97 (0.25)	6.80 (0.44)	4.91 (0.32)	5.23 (0.34)
E_{ac} (kcal/mol)	16.0	20.8	11.9	16.7	18.3
ln k_{hyb}/ln[Na^+][d]	0.99	0.56	0.76	0.61	0.48

[a] The 21-nt segment on the 3′-end of T strands is complementary to strand O.
[b] The values are hybridization rate constants at 37 °C.
[c] The number in parenthesis represents a relative rate.
[d] The k_{hyb} values were measured at 37 °C.

from the slopes. To determine activation energy (E_{ac}), the k_{hyb} values measured at different temperatures were used in Arrhenius plots as shown in Fig. 3C. In addition to the temperature dependency of the hybridization rate constant, we examined how salt concentration affects the reaction rate. The positive slope in the plot of ln k_{hyb} against ln[Na^+] shown in Fig. 3D indicates that more sodium ions are associated as the two DNA strands undergo a transition state [11,12].

Kinetic measurement and analysis were carried out for the hybridization of the five T strands with strand O to evaluate the activation energy and the change in the number of bound sodium ions (Table 2). The k_{hyb} values measured at 37 °C did not show any correlation with the length of T strands. The highest k_{hyb} value was observed with T1 and the lowest with T2. Variation in the activation energy was large; the difference in the highest (20.8 kcal/mol for T2) and the lowest (11.9 kcal/mol for T3) values was 8.9 kcal/mol. The ln k_{hyb}/ln[Na^+] values were between 0.48 (for T5) and 0.99 (for T1), indicating that transition state for the hybridization involves association of more sodium ions [11,12]. Neither E_{ac} nor ln k_{hyb}/ln[Na^+] showed a correlation with the length of T strands.

Kinetic measurement with structurally defined oligonucleotides

To eliminate ambiguity in the interpretation of kinetic data resulting from the structural dissimilarity of T strands, we used structurally defined T strands (i.e., TN strands) that were designed to examine the nucleation step with the ensuing zipping-up step unaltered. Fig. 4A shows the TN strands that were generated by removing the first 20 bases from the 5′-end of strand T1 and then attaching tandem repeats of AGTTACCC. The resulting four TN strands share an identical stem-internal loop-stem structure with an 8-base 3′-dangling end, but differing in the length of the single-stranded overhang at the 5′-end. Because the stem-internal loop-stem regions of the TN strands are not readily accessible for nucleation, the 3′-end overhang presumably serves as a nucleation site. Hybridization between strands TN and O results in an identical 21-bp duplex carrying a varying length of 5′-dangling end (note that bases in bold type in Fig. 4A comprise a segment complementary to strand O).

We examined temperature and salt dependencies of the hybridization between strands TN and O. In contrast to the hybridization between strands T and O, both activation energy and ln k_{hyb}/ln[Na^+] values show linear relationships with the length of the 5′-dangling end (Fig. 4B and C). Secondary structure prediction with mfold shows that the 5′-dangling ends for all TN strands do not form any stable intramolecular secondary structure, indicating that the 5′-dangling end remains as a single-stranded state during the hybridization reaction. Therefore, Fig. 4 indicates that the 5′-dangling end affects the activation energy and the number of bound sodium ions in a length-dependent manner.

Discussion

Fluorescent methods have been popularly employed in kinetic and thermodynamic analysis of nucleic acid hybridization owing to the high-sensitivity quantitation and a wide range of fluorophores. In addition to the presence of a nearby fluorophore that can absorb the emission energy through resonance energy transfer, changes in a local chemical environment such as neighboring hydrophobic species are also known to influence the fluorescence intensity [25]. This property has been extensively used to monitor protein folding using internal tryptophan fluorescence [26–29]. This led us to envision that a single fluorophore labeled on either of two complementary oligonucleotides could be used to monitor hybridization reaction, because the number of nucleotides available for interaction with the fluorophore should be altered depending on the hybridization state. In this study, we placed a fluorescent probe opposite to a predesigned nucleation site in strand O to detect the final hybridization product (i.e., TN–O complex) selectively over hybridization intermediates.

Oligonucleotides usually adopt intramolecular secondary structures depending on the length. Therefore, hybridization between such structured oligonucleotides involves disruption of pre-exist-

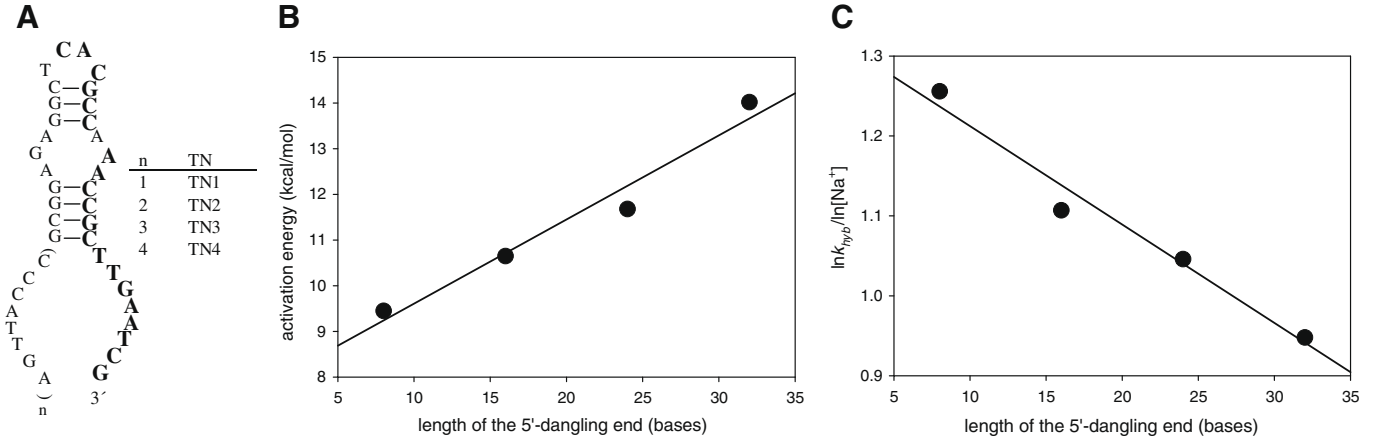

Fig. 4. Kinetic analysis of the hybridization reaction with strands TN and O. (A) Secondary structures of TN strands predicted by mfold. Bases in bold type are complementary to strand O. The lowercase n represents the number of repeating units at the 5′-dangling end. Effect of the length of 5′-dangling end on (B) activation energy and (C) change in the number of bound sodium ion during a rate-determining step.

ing secondary structure by newly formed intermolecular base pairing, following formation of a nucleation complex. The intramolecular secondary structures are thought to affect both nucleation and zipping-up steps, which is one of the reasons why considering the secondary structure effect in the analysis of kinetic data remains challenging. In this study, neither activation energy nor $\ln k_{hyb}/\ln[Na^+]$ values turned out to correlate with the length of strand T as shown in Table 2, suggesting that pre-existing secondary structure plays a pivotal role in determining the hybridization rate. However, it was practically impossible to interpret the kinetic data in Table 2 in terms of secondary structures of strands T shown in Figure S1, because the T strands do not have a structural similarity. Another problem in analyzing the kinetic data was that nucleation can occur anywhere within strand O and the 3′-end 21-base segment of strand T. Considering that the fluorescence signal is influenced by local hybridization state of 3′-end of strand O, the k_{hyb} value obtained from the kinetic trace is a mean value averaged over different reaction pathways starting at a varying nucleation site.

To remove such ambiguity arising from structural dissimilarity, we designed TN strands that share an identical secondary structure with a defined nucleation site. The only difference is the length of a dangling end located distally from the putative 3′-end nucleation site. Therefore, once the nucleation complex is formed, TN strands are likely to follow the same displacement pathway involving disruption of pre-existing secondary structures and formation of new base pairing. Because the 5′-dangling end in strand TN was designed not to form any stable secondary structure, we expected that the 5′-dangling end would hinder formation of the nucleation complex occurring at the 3′-end overhang in a length-dependent manner.

Intriguingly, we observed that activation energy is linearly proportional to the length of the 5′-dangling end (Fig. 4B), generating a 0.18 kcal/mol energy barrier per nucleotide. To our knowledge, this is the first demonstration of the length-dependent linear increase in activation energy caused by a single-stranded region flanking the nucleation site. One of the possible explanations for the linear relationship is that the timespan involved in a searching process for the nucleation site in strand O to find a perfect counterpart in strand TN is seemingly proportional to the length of the 5′-dangling end that extends the searching process by forming non-productive base pairing with strand O. It is likely that the initial encounter complex would keep forming and breaking transient base pairing between non-complementary segments until the nucleation complex is formed [9]. The free energy required to break the transient base pairing adds up to the activation energy, presumably contributing to a substantial energy barrier even for the hybridization between unstructured oligonucleotides [11–13].

The linear relationship between the length of the 5′-dangling end and $\ln k_{hyb}/\ln[Na^+]$ value was an unexpected result. Because the $\ln k_{hyb}/\ln[Na^+]$ value represents a change in the number of bound sodium ions during a rate-determining step [11,12], the result in Fig. 4C indicates that less sodium ions are associated in the transition state involving a longer TN strand. It is likely that a longer TN strand forms a less tight nucleation complex owing to a bigger coulombic and/or steric repulsion between the nucleation site and the 5′-dangling end, resulting in less demand for association of sodium ions to neutralize localized negative charges from DNA backbone phosphates.

In conclusion, we quantitatively determined the effect of a single-stranded segment flanking a nucleation site on the hybridization activation energy by using structurally defined oligonucleotides. Based on the results, we propose that the positive activation energy for DNA association might result from sum of the free energy required to break transient base pairing during the searching process leading to a stable nucleation complex. We expect that the results in this study may provide insights into rational selection of a target mRNA binding site for siRNA and antisense gene silencing [3,30]. For example, the presence of long single-stranded regions around a nucleation site would make the searching process exhaustive, resulting in a slow hybridization rate.

Acknowledgments

This work was supported by BK21 program from the Korean Ministry of Education, start-up research funds provided by Yonsei University and Seoul R&BD Programs (NT080612, KU080657).

Appendix A. Supplementary data

Supplementary data associated with this article can be found, in the online version, at doi:10.1016/j.bbrc.2009.04.140.

References

[1] V.A. Bloomfield, D.M. Crothers, I. Tinoco, Nucleic Acids: Structure, Properties and Functions, University Science Books, Sausalito, CA, 2000.
[2] F.A. Aldaye, A.L. Palmer, H.F. Sleiman, Assembling materials with DNA as the guide, Science 321 (2008) 1795–1799.
[3] G. Meister, T. Tuschl, Mechanisms of gene silencing by double-stranded RNA, Nature 431 (2004) 343–349.
[4] W. Reisner, N.B. Larsen, H. Flyvbjerg, J.O. Tegenfeldt, A. Kristensen, Directed self-organization of single DNA molecules in a nanoslit via embedded nanopit arrays, Proc. Natl. Acad. Sci. USA 106 (2009) 79–84.
[5] Q. Xu, M.R. Schlabach, G.J. Hannon, S.J. Elledge, Design of 240,000 orthogonal 25mer DNA barcode probes, Proc. Natl. Acad. Sci. USA 106 (2009) 2289–2294.
[6] B. Dubertret, M. Calame, A.J. Libchaber, Single-mismatch detection using gold-quenched fluorescent oligonucleotid, Nat. Biotechnol. 19 (2001) 365–370.
[7] T. Heyduk, E. Heyduk, Molecular beacons for detecting DNA binding proteins, Nat. Biotechnol. 20 (2002) 171–176.
[8] C. Chen, W. Wang, Z. Wang, F. Wei, X.S. Zhao, Influence of secondary structure on kinetics and reaction mechanism of DNA hybridization, Nucleic Acids Res. 35 (2007) 2875–2884.
[9] X. Chen, Y. Zhou, P. Qu, S.Z. Xin, Base-by-base dynamics in DNA hybridization probed by fluorescence correlation spectroscopy, J. Am. Chem. Soc. 130 (2008) 16947–16952.
[10] Y. Gao, L.K. Wolf, R.M. Georgiadis, Secondary structure effects on DNA hybridization kinetics: a solution versus surface comparison, Nucleic Acids Res. 34 (2006) 3370–3377.
[11] W.H. Braunlin, V.A. Bloomfield, 1H NMR study of the base-pairing reactions of d(GGAATTCC): Salt effects on the equilibria and kinetics of strand association, Biochemistry 30 (1991) 754–758.
[12] W.H. Braunlin, V.A. Bloomfield, 1H NMR study of the base-pairing reactions of d(GGAATTCC): Salt and polyamine effects on the imino proton exchange, Biochemistry 27 (1988) 1184–1191.
[13] L.E. Morrison, L.M. Stols, Sensitive fluorescence-based thermodynamic and kinetic measurements of DNA hybridization in solution, Biochemistry 32 (1993) 3095–3104.
[14] L.J. Parkhurst, Kinetic studies by fluorescence resonance energy transfer employing a double-labeled oligonucleotide: Hybridization to the oligonucleotide complement and to single-stranded DNA, Biochemistry 34 (1995) 285–292.
[15] H. Urata, H. Shimizu, H. Hiroaki, D. Kohda, M. Akagi, Thermodynamic study of hybridization properties of heterochiral nucleic acids, Biochem. Biophys. Res. Commun. 309 (2003) 79–83.
[16] S.A. Kushon, J.P. Jordan, J.L. Seifert, H. Nielsen, P.E. Nielsen, B.A. Armitage, Effect of secondary structure on the thermodynamics and kinetics of PNA hybridization to DNA hairpins, J. Am. Chem. Soc. 123 (2001) 10805–10813.
[17] T. Ohmichi, H. Nakamuta, K. Yasuda, N. Sugimoto, Kinetic property of bulged helix formation: analysis of kinetic behavior using nearest-neighbor parameters, J. Am. Chem. Soc. 122 (2000) 11286–11294.
[18] G. Bonnet, S. Tyagi, A. Libchaber, F.R. Kramer, Thermodynamic basis of the enhanced specificity of structured DNA probes, Proc. Natl. Acad. Sci. USA 96 (1999) 6171–6176.
[19] A. Tsourkas, M.A. Behlke, G. Bao, Hybridization of 2′O-methyl and 2-deoxy molecular beacons to RNA and DNA targets, Nucleic Acids Res. 30 (2002) 5168–5174.
[20] A. Tsourkas, M.A. Behlke, S.D. Rose, G. Bao, Hybridization kinetics and thermodynamics of molecular beacons, Nucleic Acids Res. 31 (2003) 1319–1330.
[21] X. Fang, X. Liu, S. Schuster, W. Tan, Designing a novel molecular beacon for surface-immobilized DNA hybridization studies, J. Am. Chem. Soc. 121 (1999) 2921–2922.
[22] K. Tawa, W. Knoll, Mismatching base-pair dependence of the kinetics of DNA–DNA hybridization studied by surface plasmon fluorescence spectroscopy, Nucleic Acids Res. 32 (2004) 2372–2377.

[23] K. KilseJensen, H. Orum, P.E. Nielsen, B. Norden, Kinetics for hybridization of peptide nucleic acids (PNA) with DNA and RNA studied with the BIAcore technique, Biochemistry 36 (1997) 5072–5077.
[24] M. Zuker, Mfold web server for nucleic acid folding and hybridization prediction, Nucleic Acids Res. 31 (2003) 3406–3415.
[25] A. Sabahi, J. Guidry, G.B. Inamati, M. Manoharan, P. Wittung-Stafshede, Hybridization of 2-ribose modified mixed-sequence oligonucleotides: thermodynamic and kinetic studies, Nucleic Acids Res. 29 (2001) 2163–2170.
[26] M. Iwakura, T. Nakamura, C. Yamane, K. Maki, Systematic circular permutation of an entire protein reveals essential folding elements, Nat. Struct. Biol. 7 (2000) 580–585.
[27] J. Klein-Seetharaman, M. Oikawa, S.B. Grimshaw, J. Wirmer, E. Duchardt, T. Ueda, T. Imoto, L.J. Smith, C.M. Dobson, H. Schwalbe, Long-range interactions within a nonnative protein, Science 295 (2002) 1719–1722.
[28] G.S. Lakshmikanth, K. Sridevi, G. Krishnamoorthy, J.B. Udgaonkar, Structure is lost incrementally during the unfolding of barstar, Nat. Struct. Biol. 8 (2001) 799–804.
[29] S.H. Park, M.C.R. Shastry, H. Roder, Folding dynamics of the B1 domain of protein G explored by ultrarapid mixing, Nat. Struct. Biol. 6 (1999) 943–947.
[30] P.D. Zamore, B. Haley, Ribo-gnome: the big world of small RNAs, Science 309 (2005) 1519–1524.